

# Effects of nanoparticle size and content on mechanical properties of dental nanocomposites: experimental versus modeling

Hamideh Barghamadi<sup>1</sup> · Mohammad Atai<sup>2</sup> · Mohammad Imani<sup>2</sup> · Masoud Esfandeh<sup>2</sup>

Received: 31 October 2014 / Accepted: 3 August 2015 / Published online: 9 August 2015  
© Iran Polymer and Petrochemical Institute 2015

**Abstract** Mechanical properties of an experimental dental composite filled with spherical silica nanoparticles, in two different particle sizes, were investigated. The experimental results of elastic modulus and strength of the composites were compared with the prediction of models. Amorphous silica nanoparticles (ASN) with primary particle sizes of 12 nm (ASN12) and 40 nm (ASN40) were surface treated by 3-(methacryloxypropyl) trimethoxysilane ( $\gamma$ -MPS). Surface treatment of the particles was examined by FTIR spectroscopy and TGA. The composites were prepared by incorporating of the silanized ASN12 or ASN40 particles in different percentages into a mixture of 2,2-bis-[4-(2-hydroxy-3-methacryloyloxy-propoxy)phenyl]-propane (bis-GMA), triethyleneglycol dimethacrylate and a photoinitiator system. The pastes were transferred into the molds and light-cured. Diametral tensile strength (DTS), flexural strength and flexural modulus of the composites were then determined. The cross-section area of the fractured specimens and dispersion pattern of the fillers throughout the resin matrix were studied by SEM and TEM, respectively. Data were analyzed and compared using ANOVA and Tukey's HSD tests at a significance level of 0.05. An increasing trend was observed in the flexural modulus of the composites as a function of their filler content. The same trend, however, was not observed for DTS and flexural strength properties. At the same filler fraction, the nanocomposites containing ASN12 showed

significantly higher modulus than the nanocomposites filled with ASN40. The models which have been developed for prediction of modulus in the composites with rigid particle in non-rigid matrix fitted better with the experimental values.

**Keywords** Dental composites · Silica nanoparticles · Mechanical properties · Modeling

## Introduction

Dental composites have excellent esthetic properties compared to their metal-based competitors and have currently become popular dental restorative materials. The polymeric matrix of the composites is usually reinforced by incorporating of particulate and/or short fibrous fillers to improve their physical and mechanical properties [1, 2]. Particle size of the reinforcing fillers varies from a few nanometers to several micrometers [3, 4] which significantly affects mechanical properties of dental composite resins [5, 6].

The effect of particle size or volume fraction of the fillers on the flexural strength and flexural modulus of the resin-based composites have been investigated before [7–9]. The flexural properties of the composites have also been studied and predicted using analytical models [9–11]. It has been shown that incorporating of nanoparticles into dental composites may improve some properties like wear resistance, gloss retention [12], modulus [13], flexural strength, diametral tensile strength [14, 15], and fracture toughness properties [16–18]. In the composites, the main mechanism suggested for interactions occurring between the filler surface and their surrounding resin matrix is chemical bonding of the matrix monomer and the filler surface functional groups. The functional groups which present on the filler

✉ Mohammad Atai  
m.atai@ippi.ac.ir

<sup>1</sup> Department of Biomedical Engineering, Science and Research Branch, Islamic Azad University, Tehran, Iran

<sup>2</sup> Iran Polymer and Petrochemical Institute, PO Box: 14965/115, Tehran, Iran

surface are usually the methacrylates originating from the silane coupling agent bonded onto the filler surface through condensation of the silanol functional groups of prehydrolyzed silane and the hydroxyl groups on the particle surface [19].

Different models have been proposed to predict the effect of parameters such as filler particle size, filler geometry and shape, interfacial interactions, etc. on the mechanical properties of composites. The models may be classified according to the characteristics of the matrix resin and/or filler [20].

Although nanoparticles have been widely used to improve the properties of polymeric matrix of dental composites [21], less attention has been devoted to compare the reinforcing effect of the particles in the nano-scale range. Therefore, the present study aims to compare the mechanical properties of experimental dental nanocomposites containing two silica nanoparticles, with 12 and 40 nm diameters, as reinforcing fillers. The amorphous silica nanoparticles were surface treated by silanization to improve interactions between the fillers and matrix resin. The effects of filler size and filler volume fraction on the mechanical properties of the composites were then investigated. The experimental results were also compared with some predicting models.

## Experimental

### Materials

2,2'-Bis-[4-(2-hydroxy-3-methacryloyloxy-propoxy)phenyl]-propane (bis-GMA) and triethyleneglycol dimethacrylate (TEGDMA) were prepared from Evonik (Germany). Camphor quinone (CQ), *N-N'*-dimethylaminoethyl methacrylate (DMAEMA), and 3-(methacryloxy)propyl trimethoxy silane ( $\gamma$ -MPS) were procured from Sigma-Aldrich (Germany). Amorphous, fumed silica with a primary particle size of 12 nm (surface area of 200 m<sup>2</sup>/g, Aerosil<sup>®</sup> 200, ASN12 in abbreviation) and 40 nm (surface area of 50 m<sup>2</sup>/g, Aerosil<sup>®</sup> OX50 ASN40, in abbreviation) in diameter were obtained from Evonik (Germany). Acetic acid was purchased from Merck (Germany).

### Methods

#### Preparation of the nanocomposites

The ASN12 and ASN40 were surface treated by silanization in the presence of 5 and 10 wt%  $\gamma$ -MPS, respectively.  $\gamma$ -MPS was prehydrolyzed for 0.5 h in an aqueous solution of ethanol (70 wt%). The pH of ethanol solution was adjusted to 3–4 using acetic acid. The fillers were added to

**Table 1** The composition of the experimental composites

Groups	Inorganic phase (wt%)	Strain-at-break $\pm$ SD <sup>a</sup>
Composite-containing ASN12		
A1	0	0.048 $\pm$ 0.013
A2	15	0.037 $\pm$ 0.003
A3	20	0.032 $\pm$ 0.006
A4	25	0.023 $\pm$ 0.006
A5	30	0.016 $\pm$ 0.003
Composite-containing ASN40		
O1	25	0.047 $\pm$ 0.013
O2	35	0.034 $\pm$ 0.010
O3	45	0.026 $\pm$ 0.004
O4	50	0.019 $\pm$ 0.004
O5	53	0.017 $\pm$ 0.003

<sup>a</sup> SD Standard deviation

the solution and left for 1 week at room temperature. The fillers were separated, washed with ethanol, and dried. The nanoparticles were then incorporated into the matrix phase (a mixture of bis-GMA/TEGDMA, 70/30 wt/wt) and ethanol as solvent. The nanoparticles were thoroughly mixed and sonicated to obtain a homogeneous suspension. The solvent was then evaporated under reduced pressure to produce a homogeneous paste. Afterwards 0.5 wt% of camphor quinone and 0.5 wt% *N-N'*-dimethylaminoethyl methacrylate, respectively, as photoinitiator and accelerator, were dissolved in the paste under sub-ambient light. The compositions of the nanocomposites are tabulated in Table 1, where *A* represents nanocomposites containing ASN12 nanoparticles and *O* denotes nanocomposites containing ASN40 nanoparticles.

#### Diametral tensile strength (DTS)

DTS test was performed according to American National Standard Institute/American Dental Association (ANSI/ADA) specification No. 27 for light-cured resins. The nanocomposite pastes were inserted into cylindrical stainless-steel molds with an internal diameter of 6 mm and height of 3 mm and cured for 40 s from both sides using a light-curing unit (LE Demetron, Kerr Corp., USA). The specimens were removed from the mold and stored in artificial saliva for 1 day at 37 °C prior to the test. A universal testing machine (UTM 2, Azmoon Gostar Co., Iran) was utilized for the test at a cross-head speed of 10 mm.min<sup>-1</sup> (seven repeats). The DTS (MPa) was then calculated according to the following equation:

$$DTS = 2P/\pi DL, \quad (1)$$

where *P* is the load at fracture (N), *D* (mm) and *L* (mm) are diameter and height of specimens, respectively.

### Flexural strength (FS) and flexural modulus (FM)

Flexural strength (FS) of the nanocomposites was determined according to the ISO specification No.4049/2000 [22] for polymer-based restorative materials which is widely employed in dental research [23, 24]. To this end, rectangular-shaped specimens (2 mm × 2 mm × 25 mm) (seven repeats) were prepared in stainless-steel molds. An overlapping regime was applied during photo-irradiation to the whole specimens on both sides (40 s for each irradiation). All specimens were stored in artificial saliva at 37 °C for 1 day prior to any further testing. The flexural strength was determined using the universal testing machine at a cross-head speed of 1 mm min<sup>-1</sup> according to the following equation:

$$FS = 3PL/2bd^2, \quad (2)$$

where  $P$  is the maximum load at the point of fracture (N),  $L$  is the span length (20 mm), and  $b$  and  $d$  are the width and thickness of the specimens in mm, respectively. The flexural modulus (FM) was also determined from the slope of the initial linear region of the stress-strain curve. The FM of the unfilled matrix resin was also measured in the same manner.

### Theoretical models

A number of theories and equations have been developed and reported to describe the elastic modulus of particulate composites. We utilized some of these equations to predict and compare the elastic modulus of our experimental nanocomposites. The equations predict the modulus based on the volume fraction of the ingredients. Therefore, the volume fraction of the fillers and the matrix phase of the nanocomposites were calculated according to the following equation [25]:

$$V_f = W_f / \left[ W_f + \left( \frac{\rho_f}{\rho_m} \right) (1 - W_f) \right], \quad (3)$$

where  $v_f$ ,  $w_f$  and  $\rho_f$  are the volume fraction, weight fraction, and density of the filler, respectively, and  $\rho_m$  is density of the matrix. The density of the fillers was 2.2 g cm<sup>-3</sup> and density of the matrix was determined as 1.13 g cm<sup>-3</sup> considering density of bis-GMA (1.16 g cm<sup>-3</sup>) and TEGDMA (1.075 g cm<sup>-3</sup>) [10] and their volume fraction according to the “rule of mixtures”.

### Scanning electron microscopy (SEM)

The fractured surfaces of the specimens were examined for determining the mode of fracture using Evo<sup>®</sup> 40 (Zeiss, UK) scanning electron microscopy. The samples were gold-coated by a sputter coater (INCA x-sight, polaron SC 7620, UK) prior to SEM observations.

### Transmission electron microscope (TEM)

Transmission electron microscopy (Philips, CM30, The Netherlands) was used to observe dispersion pattern of the particles. Ultramicrotomy was performed at room temperature (OmU3, Reichert, Austria) for sample preparation. The layer was placed on a carbon-coated copper grid for TEM observations.

### Fourier-transform infrared (FTIR) spectroscopy

FTIR spectroscopy (Bruker, Vertex 80, Germany) was performed to characterize the silanized fumed silica nanoparticles. The nanoparticles were mixed with KBr powder in 1:100 weight ratio. Aliquots of the mixture were compressed to form discs (10 mm dia.). The infrared spectra of discs were collected on FTIR spectrometer at 4 cm<sup>-1</sup> resolution and 16 scans.

### Thermal gravimetric analysis (TGA)

The extent of silane grafting on the fumed silica fillers surface was measured by thermogravimetric analysis (TGA/DSC1, Mettler Toledo, Switzerland) at a heating rate of 10 °C min<sup>-1</sup> under nitrogen atmosphere.

### Statistical analysis

The results were analyzed and compared using one-way ANOVA and the Tukey's test at the significance level of 0.05. The reported values are at least the average of seven independent measurements for mechanical tests.

## Results and discussion

The effects of particle size and volume fraction of the fillers on the mechanical properties of composites have already been reported in the literature [1, 2]. The studies have mostly focused on micron-sized particles. Characterizing and modeling of the mechanical properties of nanocomposites have attracted considerable attention due to the unique properties of the composites [26]. Therefore, this study focuses on the mechanical properties of nanocomposites and their modeling.

### Surface treatment

An agglomeration of nanoparticles may end up in micrometric particles. The formation of these micrometer-sized agglomerates is a cause for deteriorating the mechanical properties. The particles thus need surface modification to reduce clustering and improve their dispersion throughout

**Fig. 1** FTIR spectra of modified and unmodified silica nanoparticles (ASN12)

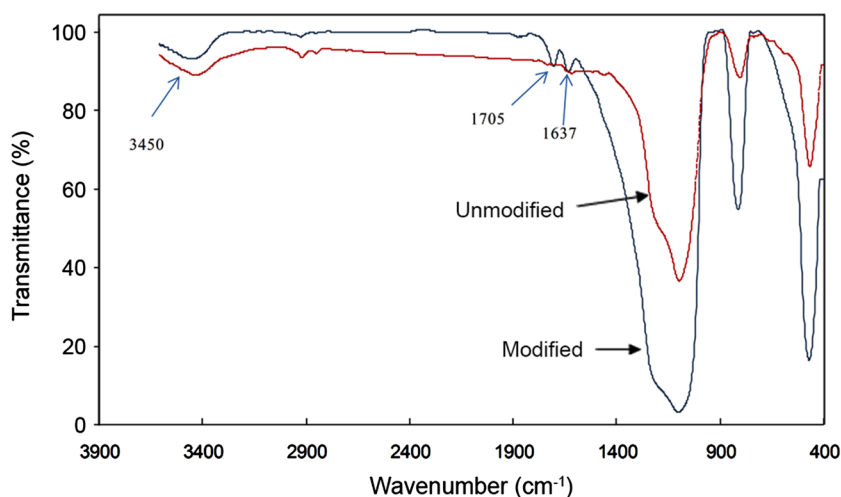
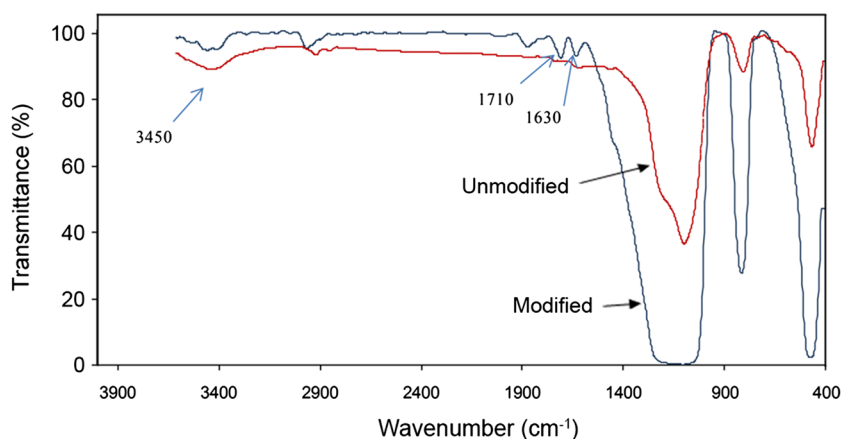


**Fig. 2** FTIR spectra of modified and unmodified silica nanoparticles (ASN40)



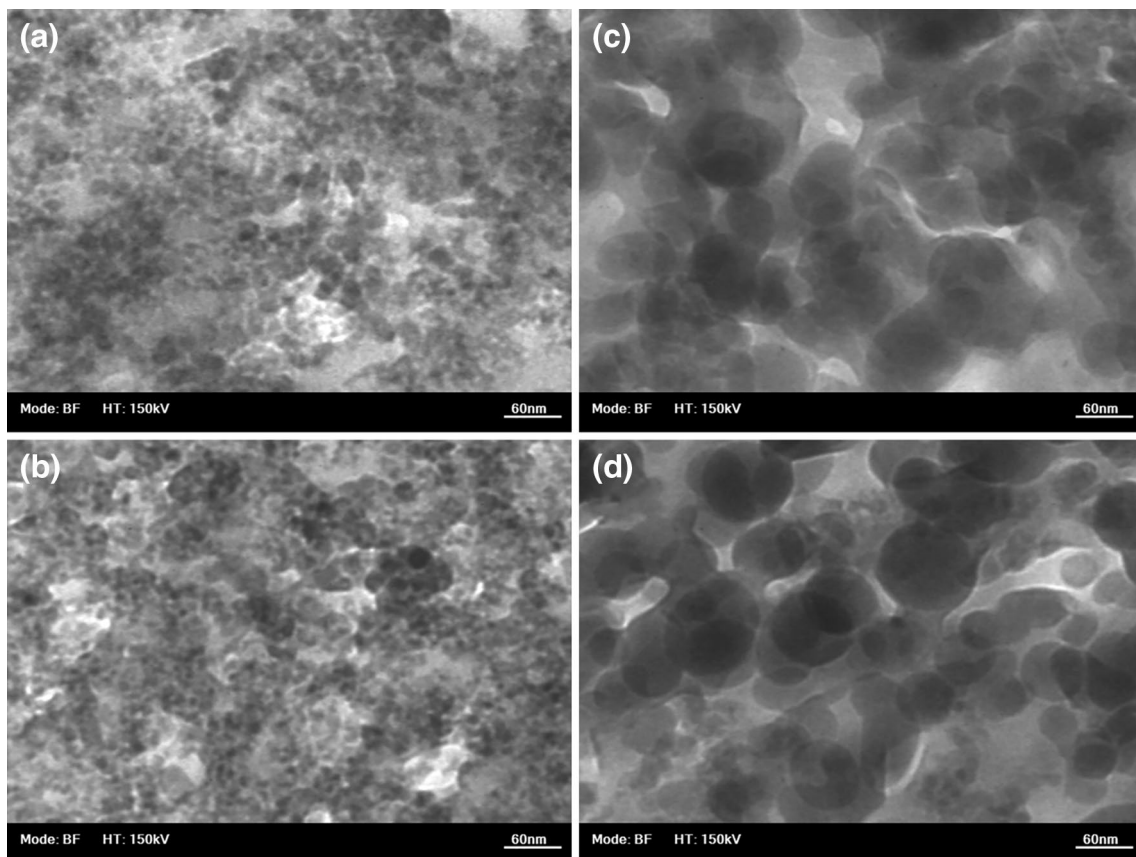
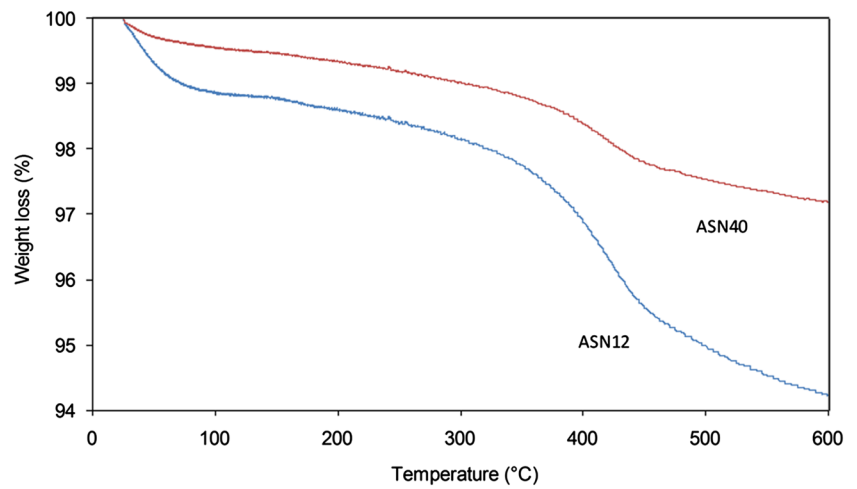
the resin matrix. In dentistry, silica nanoparticles are usually preferred because of their high biocompatibility and pleasing tint [27].

After treating with  $\gamma$ -MPS, the surface functionalized particles were characterized by FTIR spectroscopy. Figures 1 and 2 represent FTIR spectra of the modified and unmodified silica nanoparticles (ASN12 and ASN40, respectively). Both spectra confirm silanization of the nanoparticles. Grafting of  $\gamma$ -MPS onto the silica nanoparticles provides a new peak appeared in the range of 1705–1710  $\text{cm}^{-1}$  due to the stretching vibration of carbonyl groups originating from  $\gamma$ -MPS. The reaction chemically begins with the hydrolysis of the OH groups of  $\gamma$ -MPS into silanols (Si-OH) which can condense with OH functional groups positioned on the silica surface forming siloxane bonds. A  $\gamma$ -MPS surface layer on the silica nanoparticles encourages better dispersion within the resin matrix. The emerging peak positioned at 1630–1637  $\text{cm}^{-1}$  is also attributed to the methacrylate double bond of  $\gamma$ -MPS.

The extent of silanization of the nanoparticles was investigated by TGA as shown in Fig. 3. In the TGA

curves the weight loss up to 200  $^{\circ}\text{C}$  is due to the evaporation of physically adsorbed water. The further weight loss between 200 and 600  $^{\circ}\text{C}$  is due to the thermal degradation of the organic modifier and was considered as the silane grafting percentage. Figure 3 shows that 2.0 and 4.5 % weight losses occur for ASN40 and ASN12 nanoparticles, respectively. ASN12 nanoparticles possess higher surface area than ASN40 and, consequently, more hydroxyl functional groups for bonding with  $\gamma$ -MPS. So, the extent of  $\gamma$ -MPS functionalization at the surface of ASN12 is more than the ASN40.

TEM images of the nanocomposites are also shown in Fig. 4. In panels (a) and (b) nanocomposites with 15 and 30 wt% of ASN12 nanoparticles and in panels (c) and (d), nanocomposites with 50 and 53 wt% of ASN40 nanoparticles are shown. TEM imaging showed good dispersion of the fillers in the resin matrix. The interface effect in nanocomposites is more important than in composites containing micron-sized filler, due to the higher specific surface area of the nanoparticulate fillers [1]. Chemical coupling agents can influence dispersion and improve

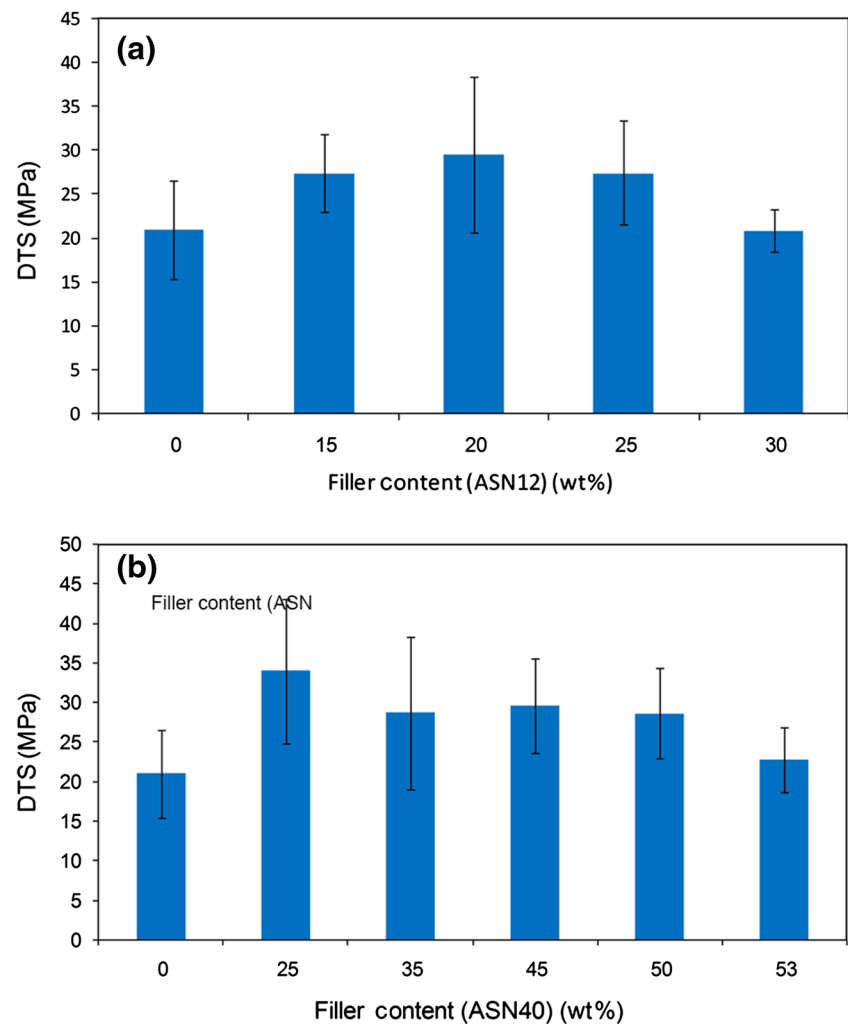
**Fig. 3** TGA curves of silanized nanoparticles**Fig. 4** TEM images of group of composites: A2 (a), A5 (b), O4 (c) and O5 (d)

bonding between inorganic nanoparticles and the resin matrix [28]. The agglomerates, however, still form, as shown in TEM images, i.e., Figure 4. Since, ASN12 nanoparticles are smaller in size than ASN40; they possess higher specific surface area and surface energy resulting in more agglomerates. This phenomenon is recognizable in panels (a) and (b).

### Mechanical properties

DTS of dental composites depends on the filler content [29]. In general, the enhancement in DTS can be achieved when the particles are well bonded to the resin matrix. Figure 5 shows diametral tensile strength of the composites with no significant differences between nanocomposites of

**Fig. 5** Diametral tensile strength (DTS) of composites containing different filler contents: **a** ASN12 and **b** ASN40



different compositions ( $p > 0.05$ ). However, increasing in the silica filler content beyond the optimal value (20 wt% in nanocomposites containing of ASN12 and 25 wt% in nanocomposites containing of ASN40) resulted in reduced DTS. The findings are in accordance with those of Ekworapoj et al. [29] report. They reported that the composites showed better strength at lower filler content. Figure 6 depicts flexural strength of the nanocomposites. According to the results, flexural strength of the neat resin specimen and nanocomposites containing ASN12 were not different ( $p > 0.05$ ), while flexural strength of the neat resin and the specimens containing ASN40 filler are significantly different ( $p < 0.05$ ). The chemical bonding of the silane coupling agent,  $\gamma$ -MPS, prevents the crack propagation through the filler–matrix interface resulting in higher flexural strength. The flexural strength in nanocomposites containing ASN40 increases at higher rate than that of nanocomposites containing of ASN12. Figures 7 and 8 show flexural modulus of the nanocomposites. The results in these figures are summarized in Table 2. The statistical comparison between

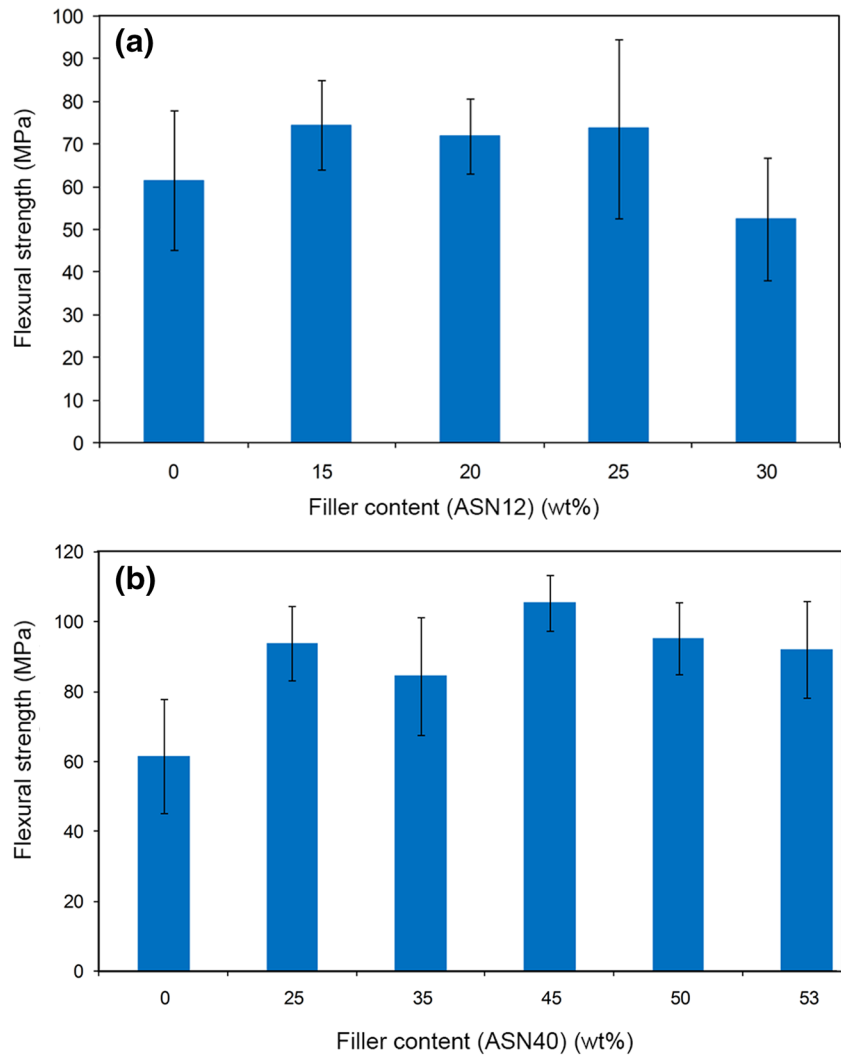
the nanocomposites from the same category (ASN40 or ASN12) showed a statistically significant ( $p < 0.05$ ) difference in flexural modulus due to the varying filler content. The elastic modulus of a particulate–polymer composite is generally determined by the elastic properties of its particle and matrix components [30]. Since the inorganic particulate fillers generally have higher stiffness, the modulus of the polymeric matrix of dental composites is improved by incorporation of the rigid fillers.

SEM micrographs of the fractured surface of the specimens are shown in Fig. 9. This figure illustrates the details on the surface of the fractured specimens. The smooth surface without any remnant is representative of a brittle fracture.

#### Prediction of the elastic modulus

According to the rigidity of the particle and matrix, the models might be categorized in two classes: rigid particles in non-rigid matrix and rigid particles in rigid matrix [20].

**Fig. 6** Flexural strength of the composites containing different filler contents: **a** ASN12 and **b** ASN40



In the following, the experimental results of elastic modulus are fitted to the models and compared. The good of fitness is reported by the  $R$  square of the least square analysis.

#### Models for rigid particles in non-rigid matrices

Einstein's equation for prediction of the Young's modulus of particulate composite is [31] as follows:

$$\frac{E_c}{E_m} = 1 + 2.5V_f, \quad (4)$$

where  $E_c$  and  $E_m$  are Young's modulus of composite and matrix, and  $V_f$  is particle volume fraction. As Figs. 7 and 8 show the prediction of the modulus of the nanocomposites by Einstein's equation is far from the experimental values ( $R^2 = 0.09$ ). Einstein's equation was originally derived for the effective shear viscosity of dilute suspensions of rigid spheres and was extended to study the effective viscosity of concentrated suspensions of mono-sized spheres [32].

Guth [33] added a particle interaction term in the Einstein's equation as follows:

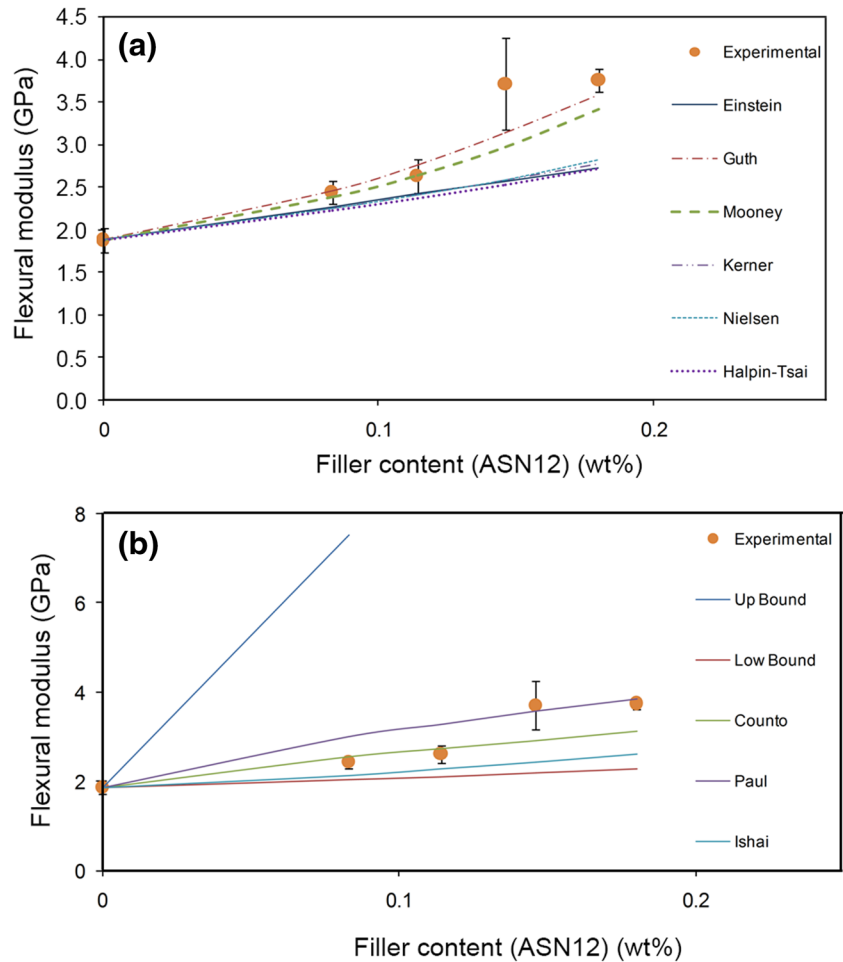
$$\frac{E_c}{E_m} = 1 + 2.5V_f + 14.1V_f^2, \quad (5)$$

where the linear term is the stiffening effect of individual particles and the second power term stands for contribution of the particles interaction. The Guth prediction is in agreement with the experimental data ( $R^2 = 0.86$ ) (Fig. 7; Table 2). Halpin and Tsai found that the modulus of particulate composites can be predicted by a semi-empirical relationship [4, 34]:

$$\frac{E_c}{E_m} = \frac{1 + ABV_f}{1 - BV_f}, \quad (6)$$

where  $A$  and  $B$  are constants for a given composite.  $A$  is a function of the particle shape and matrix Poisson's ratio, and  $B$  is related to the modulus of the particle ( $E_p$ ) and matrix ( $E_m$ ).

**Fig. 7** The experimental elastic modulus and the model prediction for ASN12 nanocomposites: **a** models for rigid particles in non-rigid matrix and **b** models for rigid particles in rigid matrix



$$A = K_E - 1, \tag{7}$$

where  $K_E$  is Einstein’s coefficient.

$$B = \frac{\frac{E_f}{E_m} - 1}{\frac{E_f}{E_m} + A} \tag{8}$$

Another equation for estimating the modulus of a composite, containing spherical particles in a matrix, proposed by Kerner [35]:

$$\frac{E_c}{E_m} = 1 + \left[ \frac{V_f}{1 - V_f} \frac{15(1 - \nu_m)}{8 - 10\nu_m} \right] \tag{9}$$

where  $\nu_m$  is the Poisson’s ratio of matrix. Poisson’s ratio was considered as  $\nu_m = 0.35$  in the present study [36]. The prediction of the Kerner equation does not cover the experimental values (Figs. 7, 8). Nielsen [34, 37, 38] used Eqs. (6) and (7) and suggested the following equation:

$$\frac{E_c}{E_m} = \frac{1 + ABV_f}{1 - \psi BV_f}, \tag{10}$$

where  $\psi$  is related to particle packing fraction and constants  $A$  and  $B$  are as described before. The factor  $A$  is calculated as  $A = 1.168$  for our experimental nanocomposites ( $K_E = 2.168$  as suggested in the Ref. [38] for a matrix with Poisson’s ratio of 0.35). The elastic modulus of fillers may be considered as  $E_f = 70$  GPa [39]

$$\psi = 1 + \frac{(1 - \varphi_m)V_f}{\varphi_m^2}. \tag{11}$$

The factor  $\varphi$  is related to the maximum packing fraction of the filler. For the studied systems with nearly spherical particles (aspect ratio of the particles is close to 1.0), a random close packing with  $\varphi = 0.63$  [20, 38] was considered. The Nielsen’s equation prediction is found lower than the experimental values (Figs. 7, 8). Mooney [40] suggested another modification to the Einstein’s equation as follows:

$$\frac{E_c}{E_m} = \exp\left(\frac{2.5V_f}{1 - sV_f}\right), \tag{12}$$

where  $s$  is a crowding factor (the ratio of the apparent volume occupied by the filler to its true volume). For close



**Fig. 8** The experimental elastic modulus and the model prediction for ASN40 nanocomposites: **a** models for rigid particles in non-rigid matrix and **b** models for rigid particles in rigid matrix

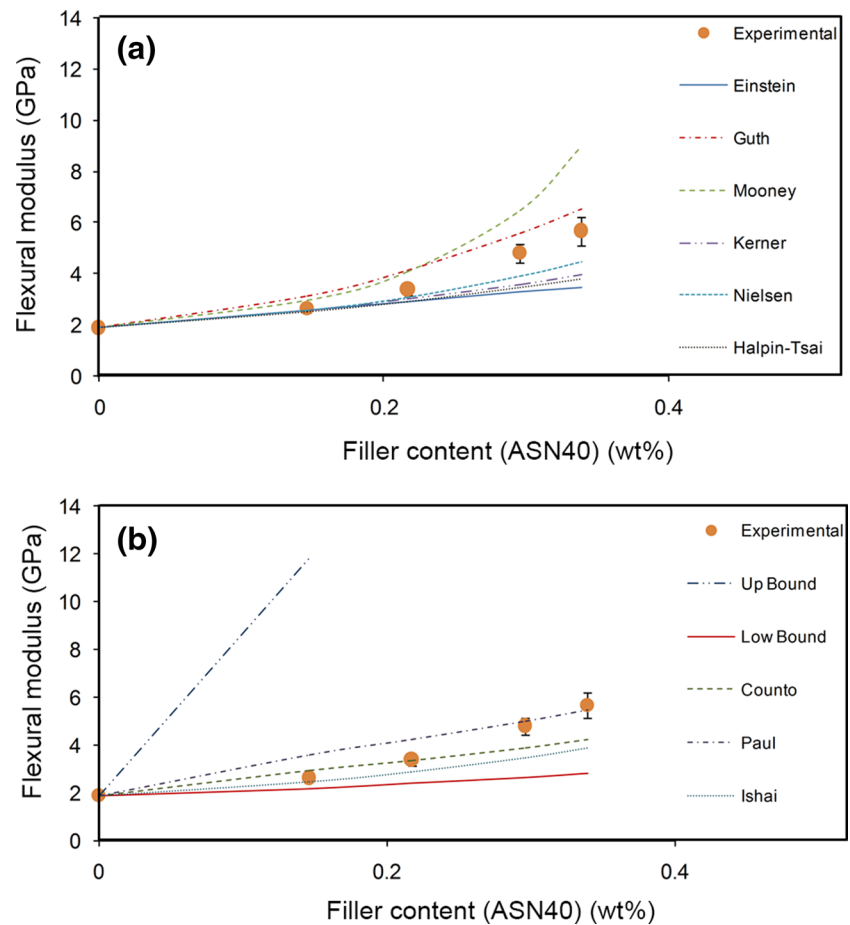


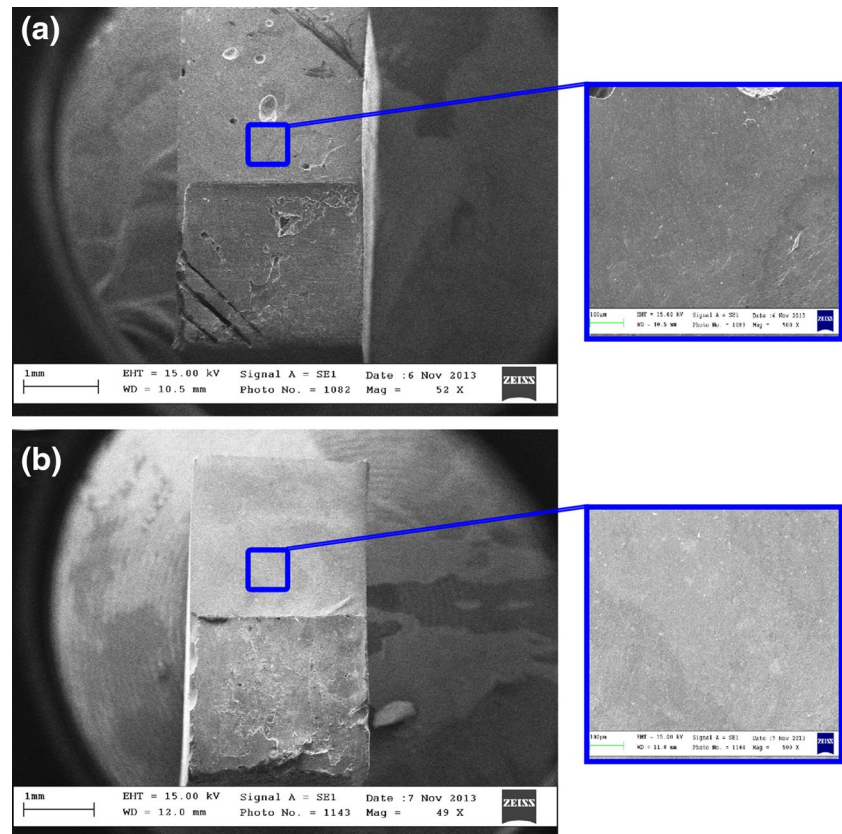
**Table 2** The experimental and predicted elastic modulus (GPa) using different models

Groups	Experimental modulus (GPa)	Einstein	Guth	Mooney	Kerner	Nielsen	Halpin-Tsai	Counto	Paul	Ishai
Composite-containing ASN12										
A1	1.88	1.88	1.88	1.88	1.88	1.88	1.88	1.88	1.88	1.88
A2	2.43	2.27	2.45	2.37	2.24	2.24	2.22	2.55	3.01	2.14
A3	2.62	2.41	2.76	2.63	2.40	2.40	2.37	2.73	3.28	2.28
A4	3.71	2.56	3.13	2.96	2.57	2.58	2.53	2.92	3.56	2.44
A5	3.75	2.72	2.71	3.40	2.77	2.81	2.71	3.12	3.86	2.62
Composite-containing ASN40										
O1	2.62	2.56	3.13	2.96	2.57	2.58	2.53	2.92	3.56	2.44
O2	3.39	2.89	4.14	4.04	3.00	3.09	2.92	3.35	4.20	2.86
O3	4.79	3.27	5.59	6.44	3.58	3.88	3.45	3.89	4.98	3.46
O4	5.67	3.47	6.51	8.97	3.96	4.47	3.79	4.23	5.45	3.87
O5	6.20	3.60	7.17	11.58	4.23	4.94	4.03	4.46	5.78	4.16

packed spheres  $s$  is equal 1.35 [20]. This model predicts values close to the experimental data ( $R^2 = 0.74$ ). The Mooney equation predicts considerably more reinforcing efficiency than the Kerner equation and a modulus that tends to infinity at high volume fraction of filler. The equation assumes that  $\nu_m = 0.5$  and that the modulus of the filler

is infinitely greater than the matrix, both of which are not correct for a rigid matrix thus restricting the applicability of this model for filled rigid thermosetting polymeric matrices [20, 38]. According to Fig. 8, the prediction of Halpin-Tsai equation is not in agreement with the experimental values ( $R^2 = 0.04$ ).

**Fig. 9** SEM micrographs of the fracture surface of groups A4 (a) and O1 (b)



### Models for rigid particle in rigid matrices

Voigt and Reuss calculated the effective modulus in fiber composites in the fiber direction and in the transverse direction, respectively, as [26, 41] follows:

$$E_c^L = E_m V_f + E_m (1 - V_f) \quad (13)$$

and

$$E_c^T = \frac{E_f E_m}{[E_f (1 - V_f) + E_m V_f]}, \quad (14)$$

where  $V_f$  is the volume fraction of fiber and  $E_f$  and  $E_m$  represent modulus for fiber and matrix, respectively. The superscripts  $L$  and  $T$  point to the longitudinal and transverse directions, respectively. Eqs. 13 and 14 can be used for any two-phase composites regardless of the shape of filler. Eq. 13 is also called the “rule of mixtures” and Eq. 14 is called “inverse rule of mixtures” [26]. The modulus of real composites lies between these two boundaries. These equations are upper- and lower-bound models and are applicable to particulate micro- and nanocomposites. Generally, the modulus of composites should be lower than upper-bound predicted by Eq. 13 and higher than the lower-bound by Eq. 14 [26, 42]. For two-phase materials Counto [43] proposed a simple model by assuming perfect

bonding between filler and matrix. The composite modulus is given by

$$\frac{1}{E_c} = \frac{1 - V_f^{\frac{1}{2}}}{E_m} + \frac{1}{\left[ \frac{1 - V_f^{\frac{1}{2}}}{V_f^{\frac{1}{2}}} \right] E_m + E_f} \quad (15)$$

This model predicts moduli in good agreement with a wide range of testing data. Ishai and Cohen [44] and Paul [45] assumed that the fillers and matrix are subjected to the same uniform stress and there is a perfect adhesion between filler and matrix. When a uniform stress is applied on the boundary, the elastic modulus of the particulate composite is given by

$$\frac{E_c}{E_m} = 1 + \frac{1 + (k - 1) V_f^{2/3}}{1 + (k - 1) (V_f^{2/3} - V_f)}, \quad (16)$$

which is another upper-bound solution. Using the same model, with uniform strain applied at the boundary, Ishai and Cohen [44] obtained a lower-bound solution:

$$\frac{E_c}{E_m} = 1 + \frac{V_f}{\frac{K}{K-1} - V_f^{1/3}} \quad (17)$$

where  $K = E_f/E_m$ .

The predicted and experimental results (Figs. 7, 8) indicate that there is a good agreement between experimental values and models which have been developed for rigid particles in non-rigid matrix especially that of Guth model.

### Prediction of the strength

Prediction of the strength for composite materials is difficult because it is determined by the fracture behaviors which are associated with the parameters as interface adhesion, stress concentration, and defect size/spatial distribution. Numerous theories have been developed to describe strength in composites but there is no universally accepted theory to date [26]. In the case of poor filler-matrix interface adhesion the stress cannot be transferred from the matrix to the filler. The strength of particulate-filled polymer composite is, therefore, determined from the effective sectional area of load-bearing matrix in the absence of the particles, an equation for the composite strength is [46, 47]:

$$\sigma_c = \sigma_m(1 - V_f), \quad (18)$$

where,  $\sigma_c$  and  $\sigma_m$  designate the strength of the composite and the matrix and  $V_f$  is filler volume fraction. This equation predicts that the strength of a particulate-filled composite decreases linearly with increases in filler volume fraction, but the results (Fig. 6) show an increasing trend up to the optimum filler content.

For strong particle–matrix interfacial bonding, such as the present study, Pukanszky et al. [48, 49] suggested an empirical relationship:

$$\sigma_c = \left[ \frac{(1 - V_f)\sigma_m}{1 + 2.5V_f} \right] \exp(BV_f), \quad (19)$$

where  $B$  is an empirical constant, which depends on the surface area of particles, particle density, and interfacial bonding energy [41]. Fitting to the experimental values in Eq. 19, the parameter  $B$  was calculated which was in the range of 2.3–5.4 for ASN12 and ASN40 samples, respectively. The higher value of  $B$  shows stronger interfacial adhesion between filler and matrix [49]. Figure 4 depicts a better distribution of the particles in the nanocomposite containing ASN40 in comparison with ASN12-contained nanocomposites which might be due to the formation of agglomerates of ASN12 leading to formation of local defects and weaker strength.

According to the experiments (Fig. 6), the flexural strength increased up to filler content of 14.5 vol% (25 wt%) in nanocomposites containing ASN12 nanoparticles and 29.5 vol% (45 wt%) in nanocomposites containing ASN40 nanoparticles. When the filler content increases, there would be further agglomeration which results in

weaker load transfer at the interface of filler and the matrix and reduction in flexural strength. This occurs in nanocomposites containing ASN40 by up to 29.5 vol%, which is due to the difference in particle size of the filler. The large particles do not tend to aggregate in the resin matrix [6, 8].

In nanocomposites with equal volume fraction of particles, the flexural strength increases as the particle size decreases.

### Conclusion

This study reports the effect of particle diameter and volume fraction of nanoparticles on mechanical properties (DTS, FS, FM) of spherical-silica-particle-filled composites. Particle diameters were 12 and 40 nm and the volume fraction ranged from 0 to 0.36.

The results indicate that stiffness of composite depends significantly on particle loading, since the fillers have much larger modulus than the matrix. In nanocomposites with an equal volume fraction of particles, the particle size affects flexural modulus. In this case, flexural modulus increases as the particle size is dropped.

The flexural strength increases as the volume fraction increases by up to 14.5 vol% (25 wt%) in nanocomposites containing of ASN12 and 29.5 vol% (45 wt%) in nanocomposites containing of ASN40 nanoparticles.

The predication of the theoretical values was compared with the experimental results. It can be concluded that the model which has been developed for the prediction of the modulus in the composites with rigid particle in non-rigid matrix presented a better agreement with the experimental values.

**Acknowledgments** We are grateful to Ms. Samiei and Mr. Ebrahimi in Kooshan Pars Quality Company for their expert technical assistance in mechanical analysis.

### References

1. Xia Y, Zhang F, Xie H, Gu N (2008) Nanoparticle-reinforced resin-based dental composites. *J Dentistry* 36:450–455
2. Foroutan F, Javadpou J, Atai M, Rezaie H (2011) Mechanical properties of dental composite materials reinforced with micro and nano-size  $Al_2O_3$  filler particles. *Iran J Mater Sci Eng* 8:25–33
3. Tanimoto Y, Kitagawa T, Aida M, Nishiyama N (2006) Experimental and computational approach for evaluating the mechanical characteristics of dental composite resins with various filler sizes. *Acta Biomater* 2:633–639
4. Halpin J (1969) Stiffness and expansion estimates for oriented short fiber composites. *J Compos Mater* 3:732–734
5. Mitsuhashi A, Hanaoka K, Teranaka T (2003) Fracture toughness of resin-modified glass ionomer restorative materials: effect of powder/liquid ratio and powder particle size reduction on fracture toughness. *Dent Mater* 19:747–757
6. Masouras K, Akhtar R, Watts DC, Silikas N (2008) Effect of filler size and shape on local nanoindentation modulus of resin-composites. *J Mater Sci Mater Med* 19:3561–3566

7. Junior R, Adalberto S, Zanchi CH, Carvalho RVd, Demarco FF (2007) Flexural strength and modulus of elasticity of different types of resin-based composites. *Brazil Oral Res* 21:16–21
8. Rahim T, Mohamad D, Ismail AR, Akil HM (2011) Synthesis of nanosilica fillers for experimental dental nanocomposites and their characterisations. *J Phys Sci* 22:93–105
9. Fu S-Y, Feng X-Q, Lauke B, Mai Y-W (2008) Effects of particle size, particle/matrix interface adhesion and particle loading on mechanical properties of particulate–polymer composites. *Compos Part B Eng* 39:933–961
10. Atai M, Pahlavan A, Moin N (2012) Nano-porous thermally sintered nano silica as novel fillers for dental composites. *Dent Mater* 28:133–145
11. Bourkas G, Prassianakis I, Kytopoulos V, Sideridis E, Younis C (2010) Estimation of elastic moduli of particulate composites by new models and comparison with moduli measured by tension, dynamic, and ultrasonic tests. *Adv Mater Sci Eng* 2010:891824. doi:10.1155/2010/891824
12. Mitra SB, Wu D, Holmes BN (2003) An application of nanotechnology in advanced dental materials. *J Am Dent Assoc* 134:1382–1390
13. Beun S, Glorieux T, Devaux J, Vreven J, Leloup G (2007) Characterization of nanofilled compared to universal and microfilled composites. *Dent Mater* 23:51–59
14. Ilie N, Hickel R (2009) Investigations on mechanical behaviour of dental composites. *Clin Oral Investig* 13:427–438
15. Kushch VI, Mogilevskaya SG, Stolarski HK, Crouch SL (2013) Elastic fields and effective moduli of particulate nanocomposites with the Gurtin–Murdoch model of interfaces. *Int J Solid Struct* 50:1141–1153
16. Curtis A, Palin W, Fleming G, Shortall A, Marquis P (2009) The mechanical properties of nanofilled resin-based composites: characterizing discrete filler particles and agglomerates using a micromanipulation technique. *Dent Mater* 25:180–187
17. Adachi T, Osaki M, Araki W, Kwon S-C (2008) Fracture toughness of nano- and micro-spherical silica-particle-filled epoxy composites. *Acta Mater* 56:2101–2109
18. Pukánszky B, Maurer FH (1995) Composition dependence of the fracture toughness of heterogeneous polymer systems. *Polym* 36:1617–1625
19. Antonucci JM, Dickens SH, Fowler BO, Xu HH, McDonough WG (2005) Chemistry of silanes: interfaces in dental polymers and composites. *J Res National Inst Stand Technol* 110:541–558
20. Ahmed S, Jones F (1990) A review of particulate reinforcement theories for polymer composites. *J Mater Sci* 25:4933–4942
21. Cramer N, Stansbury J, Bowman C (2011) Recent advances and developments in composite dental restorative materials. *J Dent Res* 90:402–416
22. Iso E (2000) 4049 Dentistry-polymer-based filling, restorative and luting materials. International Organization for Standardization, Geneva
23. Mirmohammadi H, Kleverlaan CJ, Feilzer AJ (2009) Rotating fatigue and flexural strength of direct and indirect resin-composite restorative materials. *Am J Dent* 22(4):219–222
24. Junior SAR, Ferracane JL, Bona ÁD (2008) Flexural strength and Weibull analysis of a microhybrid and a nanofill composite evaluated by 3- and 4-point bending tests. *Dent Mater* 24:426–431
25. Goyal R, Tiwari A, Negi Y (2008) Microhardness of PEEK/ceramic micro- and nanocomposites: correlation with Halpin–Tsai model. *Mater Sci Eng A* 491:230–236
26. Hu H, Onyebueke L, Abatan A (2010) Characterizing and modeling mechanical properties of nanocomposites—review and evaluation. *J Miner Mater Charact Eng* 9:275–319
27. Chen M-H, Chen C-R, Hsu S-H, Sun S-P, Su W-F (2006) Low shrinkage light curable nanocomposite for dental restorative material. *Dent Mater* 22:138–145
28. Mohsen N, Craig R (1995) Effect of silanation of fillers on their dispersability by monomer systems. *J Oral Rehabil* 22:183–189
29. Ekworapoj P, Magaraphani R, Martin DC (2002) Heat effect on viscosity and curing of light-cured dental resin and mechanical strength of conventional dental composites. *J Metal Mater Miner* 12:39–50
30. Zhang H, Zhang Z, Friedrich K, Eger C (2006) Property improvements of in situ epoxy nanocomposites with reduced interparticle distance at high nanosilica content. *Acta Mater* 54:1833–1842
31. Einstein A (1956) Investigations on the theory of the Brownian movement. Courier Dover Publications, USA
32. Hsueh CH, Becher PF (2005) Effective viscosity of suspensions of spheres. *J Am Ceramic Soc* 88:1046–1049
33. Guth E (2004) Theory of filler reinforcement. *J Appl Phys* 16:20–25
34. Afidi J, Kardos J (1976) The Halpin–Tsai equations: a review. *Polym Eng Sci* 16:344–352
35. Kerner EH (1956) The elastic and thermo-elastic properties of composite media. *Proc Phys Soc Sec B* 69:808
36. Nakayama WT, Hall DR, Grenoble DE, Katz JL (1974) Elastic properties of dental resin restorative materials. *J Dent Res* 53:1121–1126
37. Nielsen LE (2003) Generalized equation for the elastic moduli of composite materials. *J Appl Phys* 41:4626–4627
38. Landel RF, Nielsen LE (1993) Mechanical properties of polymers and composites. CRC Press, USA
39. Le Bourhis E (2008) Glass: mechanics and technology. Wiley, New York
40. Mooney M (1951) The viscosity of a concentrated suspension of spherical particles. *J Colloid Sci* 6:162–170
41. Fu SY, Feng XQ, Lauke B, Mai YW (2008) Effects of particle size, particle/matrix interface adhesion and particle loading on mechanical properties of particulate–polymer composites. *Composites* 39:933–961
42. Fu S-Y, Hu X, Yue C-Y (1998) A new model for the transverse modulus of unidirectional fiber composites. *J Mater Sci* 33:4953–4960
43. Counto UJ (1964) The effect of the elastic modulus of the aggregate on the elastic modulus, creep and creep recovery of concrete. *Mag Concrete Res* 16:129–138
44. Ishai O, Cohen L (1967) Elastic properties of filled and porous epoxy composites. *Int J Mech Sci* 9:539–546
45. Paul B (1959) Prediction of elastic constants of multi-phase materials. No. TR3. Brown Univ Providence, USA
46. Danusso F, Tieghi G (1986) Strength versus composition of rigid matrix particulate composites. *Polymer* 27:1385–1390
47. Levita G, Marchetti A, Lazzeri A (1989) Fracture of ultrafine calcium carbonate/polypropylene composites. *Polym Compos* 10:39–43
48. Pukánszky B, Turcsányi B, Tudos F (1988) Effect of interfacial interaction on the tensile yield stress of polymer composites. Interfaces in polymer, ceramic and metal matrix composites. Elsevier, Amsterdam, pp 467–477
49. Turcsanyi B, Pukanszky B, Tüdös F (1988) Composition dependence of tensile yield stress in filled polymers. *J Mater Sci Lett* 7:160–162